Gadolinium-Encapsulating Iron Oxide Nanoprobe as Activatable NMR/MRI Contrast Agent

Santimukul Santra,[†] Samuel D. Jativa,[†] Charalambos Kaittanis,[‡] Guillaume Normand,[‡] Jan Grimm,[‡] and J. Manuel Perez[†,*]

[†]Nanoscience Technology Center and Chemistry Department, University of Central Florida, 12424 Research Parkway, Suite 400, Orlando, Florida 32826, United States, and [‡]Department of Radiology, Memorial Sloan Kettering Cancer Center, 1275 York Avenue, New York, New York 10065, United States

ABSTRACT Herein we report a novel gadolinium-encapsulating iron oxide nanoparticle-based activatable NMR/MRI nanoprobe. In our design, Gd-DTPA is encapsulated within the poly(acrylic acid) (PAA) polymer coating of a superparamagnetic iron oxide nanoparticle (IO-PAA), yielding a composite magnetic nanoprobe (IO-PAA-Gd-DTPA) with quenched longitudinal spin−lattice magnetic relaxation (T_1). Upon release of the Gd-DTPA complex from the nanoprobe's polymeric coating in acidic media, an increase in the T_1 relaxation rate ($1/T_1$) of the composite magnetic nanoprobe was observed, indicating a dequenching of the nanoprobe with a corresponding increase in the T_1-weighted MRI signal. When a folate-conjugated nanoprobe was incubated in HeLa cells, a cancer cell line overexpressing folate receptors, an increase in the $1/T_1$ signal was observed. This result suggests that, upon receptor-mediated internalization, the composite magnetic nanoprobe degraded within the cell's lysosome acidic (pH 5.0) environment, resulting in an intracellular release of Gd-DTPA complex with subsequent T_1 activation. In addition, when an anticancer drug (Taxol) was coencapsulated with the Gd-DTPA within the folate receptor targeting composite magnetic nanoprobe, the T_1 activation of the probe coincided with the rate of drug release and corresponding cytotoxic effect in cell culture studies. Taken together, these results suggest that our activatable T_1 nanoagent could be of great importance for the detection of acidic tumors and assessment of drug targeting and release by MRI.

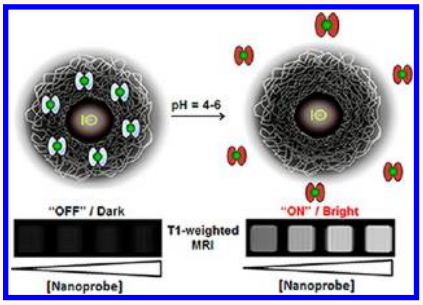

KEYWORDS: activatable MRI imaging · magnetic relaxation · iron oxide nanoprobe · Gd-DTPA complex · theranostic application

Magnetic resonance imaging (MRI) has become a powerful technique in the clinical diagnosis of disease and in animal imaging.[1−4] MRI is capable of obtaining tomographic images of living subjects with high spatial resolution as a result of perturbation of tissue water protons in the presence of an external magnetic field.[5−8] MR contrast agents[9−11] typically enhance contrast for more accurate diagnosis and most recently to allow for targeting imaging when a targeting ligand (*e.g.*, antibody, peptide) is conjugated to the MR contrast agent.[12,13] Among these agents, superparamagnetic nanoparticles[14−16] and paramagnetic metal chelates[8] are the most commonly used contrast agents.[17−21] Superparamagnetic nanoparticles are typically composed of an iron oxide nanoparticle (IONP) surrounded by a polymeric coating to facilitate increased stability in aqueous media.[22] They work by shortening the traverse relaxation time (T_2 and T_2*) of surrounding water protons, resulting in a decrease of the MR signal (negative contrast, dark signal) on a T_2-weighted MRI sequence.[23−28] On the other hand, paramagnetic gadolinium chelates create an increase in signal intensity on T_1-weighted images (positive contrast, bright signal) by shortening the longitudinal relaxation time (T_1) of surrounding water protons.[10,17,29−38]

The development of an activatable MR imaging agent that reports on a biological process associated with diseases would greatly advance medical imaging of disease at a molecular level.[39−41] Activatable T_1 or T_2 agents, those that result in modulation of either the T_1 or T_2 relaxation time upon target binding, enzymatic activity, or biological process associated with disease, would be attractive MR imaging agents, resulting in high sensitivity and high signal-to-noise ratios with low background.[20,42−48] Activatable Gd-based T_1 agents have been previously described[8,49,50] and include those designed to be biologically activated by an enzyme such as β-galactosidase[51,52] and β-glucoronidase[42,44] as well as those activated by release of a drug.[53,54] However, the lack of sufficient sensitivity and specificity and the hydrophobic nature of some of the designed probes are major problems that hamper their implementation for clinical

* Address correspondence to jmperez@ucf.edu.

Received for review May 30, 2012 and accepted July 10, 2012.

Published online July 18, 2012
10.1021/nn302393e

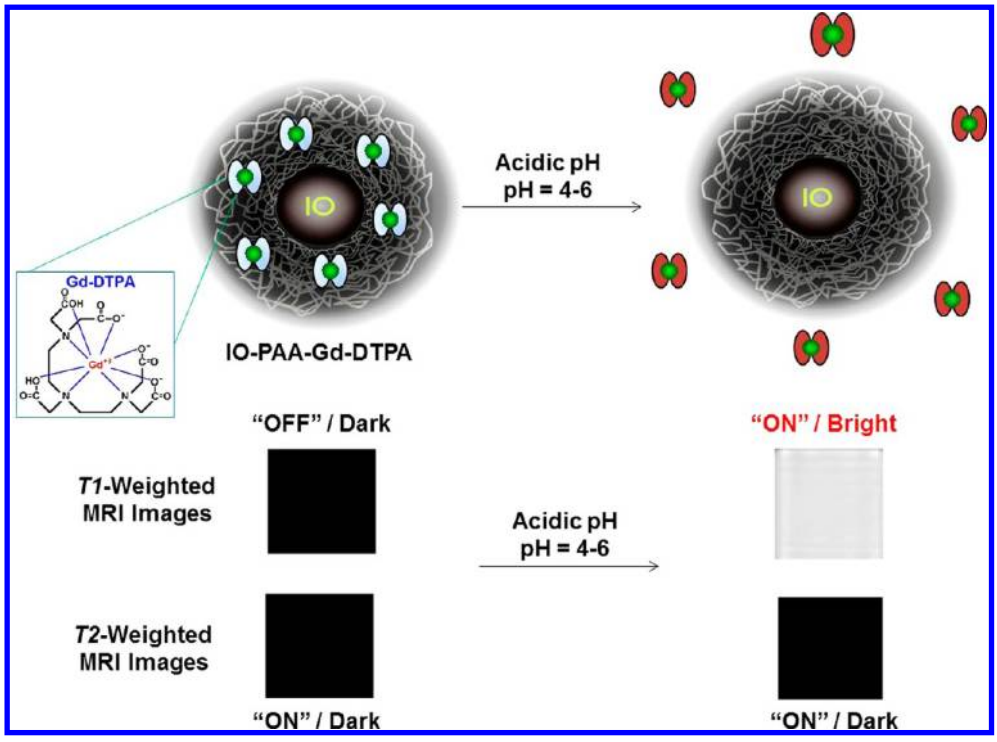

Scheme 1. Schematic representation of the acidic pH-mediated activation of the activatable composite magnetic nanoprobe IO-PAA-Gd-DTPA and corresponding T_1 MR activation. In an acidic environment, the quenched Gd-DTPA chelates are released from the iron oxide's (IO) polymeric coating, becoming activated (ON) and resulting in an enhancement in the T_1-weighted MRI image (brighter signal) and no change in the T_2-weighted image.

use. Activatable T_2 IONP-based agents are less common as it is often difficult to "quench" the strong superparamagnetic nature or magnetic moment of these nanoparticles.[26−29,55] Magnetic relaxation switches have been developed based on IONPs that cluster in the presence of a target or enzymatic activity leading to detectable changes in the T_2 relaxation times.[56−59] However, the use of these T_2 activatable agents has been difficult to implement *in vivo*, and it has so far been limited to their use as nanosensors in molecular diagnostic applications.[57,60]

An activatable T_1 agent, one that can induce a faster T_1 relaxation, would result in an increase in the T_1-weighted MR signal intensity upon target recognition for better diagnosis. Such an activatable agent could be beneficial in cancer diagnosis if it were designed to become activated upon tumor targeting, resulting in a brighter signal. Herein, we report the design, synthesis, and characterization of a new dual-mode MR contrast agent that becomes activated in an acidic environment, resulting in an increase in the T_1-weighted signal (brighter contrast). The designed MR agent is composed of superparamagnetic iron oxide nanoparticles that encapsulate Gd-DTPA chelates within the hydrophobic pockets of the nanoparticle's poly(acrylic acid) (PAA) coating (IO-PAA-Gd-DTPA). We hypothesized that the strong magnetic field induced by the large magnetic moment of the superparamagnetic iron oxide core will affect the relaxation process of the much weaker paramagnetic Gd-DTPA, resulting in quenching of its T_1 signal (Scheme 1). The superparamagnetic iron oxide core is composed of thousands of iron (Fe^{2+} and Fe^{3+}) ions magnetically ordered within the nanocrystal in such a way that they collectively create a net magnetic moment larger than that of any single paramagnetic Fe^{2+}/Fe^{3+} or Gd^{3+} ion. We then reasoned that the large magnetic moment of the iron oxide core would create a strong magnetic susceptibility in the proximity of the iron oxide core that will affect the T_1 relaxation of the Gd-DTPA encapsulated within the nanoparticle's polymeric coating. We observed that the T_1 relaxation rate ($1/T_1$) of the Gd(III)-DTPA complex was quenched (off/dark) when the Gd-DTPA complex was encapsulated within the PAA coating of the iron oxide nanoparticle (IO-PAA). Upon release of the quenched Gd-DTPA, an increase in the T_1 relaxation rate was observed with marginal increase in the T_2 relaxation rate ($1/T_2$). This quenching effect is not observed when the Gd chelate is attached to the surface of the IONP or when nonmagnetic nanoparticles, such as cerium oxide nanoparticles (NC-PAA), are used to encapsulate the Gd-DTPA. Corresponding r_1 and r_2 values for the IO-PAA-Gd-DTPA nanocomposite at different pH values revealed a pH-dependent increase in the r_1 of the nanocomposite suspension as the pH decreases, indicating T_1 activation at acidic pH. The observed pH-dependent increase in r_1 was only observed when Gd-DTPA was encapsulated within the polymeric coating of the nanoparticle but not when it was directly attached on the surface of the

nanoparticle's polymeric coating. These results confirm that indeed the superparamagnetic iron oxide nanocrystal acts as a magnetic quencher for the Gd-DTPA T_1 only when the Gd-DTPA is encapsulated within the nanoparticle's polymeric coating in close proximity to the superparamagnetic core. Furthermore, when the IO-PAA-Gd-DTPA nanocomposite was conjugated with folic acid, its selective internalization and lysosomal localization within folate-receptor-positive cells allow for selective activation due to the lysosome's acidic pH. Finally, when the folate receptor targeting nanocomposite was used to coencapsulate a cytotoxic drug (Taxol), dual delivery of the drug and T_1 imaging activation was achieved. Therefore, our newly developed activatable nanoprobe (IO-PAA-Gd-DTPA) combines features of several important modalities, such as (i) activatable T_1-weighted MRI contrast, (ii) T_2-weighted MRI contrast, (iii) receptor-targeted internalization, and (iv) delivery of anticancer drug to tumors. These features make our magnetic nanoprobe a potential MR-activatable contrast agent for cancer.

RESULTS AND DISCUSSION

Synthesis and Characterization of Gd-DTPA Composite Iron Oxide Nanoparticles. Our IO-PAA-Gd-DTPA probe was synthesized by direct addition of Gd-DTPA during the course of the IO-PAA synthesis using a modified version of our previously published protocol.[22] In brief, an aqueous solution of PAA (0.45 mmol) and Gd-DTPA (0.04 mmol) was added and mixed thoroughly before addition of a mixture of iron salts (2.26 mmol of $FeCl_3 \cdot 6H_2O$ and 1.61 mmol of $FeCl_2 \cdot 4H_2O$ in dilute HCl solution) in aqueous ammonium hydroxide solution (0.05 M). The resulting dark-brown suspension of composite IO-PAA-Gd-DTPA nanoprobe was stirred for 1 h at room temperature and then centrifuged at 4000 rpm for 30 min to get rid of free poly(acrylic acid), not encapsulated Gd-DTPA complex and other unreacted reagents. Finally, the composite nanoprobe suspension was purified using a magnetic column (Miltenyi Biotech) and washed with phosphate buffer saline (pH 7.4) solution. This *in situ* encapsulation approach proved to be effective for the encapsulation of Gd-DTPA as no change in the size and relaxivity of the nanoprobes was found over a long period of time (Supporting Information, Table S1). The encapsulation of Gd-DTPA within the nanoprobe was confirmed by measuring the amount of Gd using ICP-MS (0.289 mg Gd/mL). The amount of Fe in the IO-PAA-Gd-DTPA preparation was determined as 2.0 mg Fe/mL for a 0.05:1 Gd/Fe molar ratio. Magnetic relaxation measurements at 0.47 T of the composite nanoprobes resulted in a Gd concentration based relaxivity of $r_1 = 50.2 \pm 1.8\ mM^{-1}\ s^{-1}$ and $r_2 = 87.3 \pm 2.4\ mM^{-1}\ s^{-1}$, and $r_1 = 43.3 \pm 2.1\ mM^{-1}\ s^{-1}$ and $r_2 = 230 \pm 3\ mM^{-1}\ s^{-1}$ based on Fe concentration. These relatively high values for r_1 and r_2 might be due to the presence of both iron oxide and Gd(III) within the nanocomposite imaging probe and are comparable to reported values for high relaxivity probes.[35,40,41] Dynamic light scattering (DLS) studies indicated the presence of a stable and monodisperse suspension of nanoparticles with a hydrodynamic diameter of $D = 79 \pm 2$ nm. The diameters of these magnetic nanoprobes were further confirmed by scanning transmittance electron microscopic (STEM) experiments, which show an average diameter of 80 nm (Supporting Information, Figure S1). The synthesized IO-PAA-Gd-DTPA nanocomposite was found to be stable in PBS (pH 7.4) and serum, as no binding, clustering, or precipitations of the nanoparticles were observed over a long period of time. Similarly, the stability of the composite nanoparticles was further confirmed by observing no significant changes in magnetic relaxations, as shown in Supporting Information Table S1. Taken together, these results indicate the effective encapsulation of Gd-DTPA into the IO-PAA polymeric matrix.

pH-Dependent Activation of the Gd-DTPA Composite Magnetic Nanoprobes. We first evaluated the magnetic relaxation activation of the IO-PAA-Gd-DTPA nanoprobes in buffered solution within a pH range of 4.0 to 7.4. In these experiments, we measured the T_1 and T_2 of increasing concentrations of IO-PAA-Gd-DTPA nanoprobes at physiological (pH 7.4) and acidic (pH 4.0−6.0) buffered solutions. T_1 and T_2 readings were taken upon addition of the magnetic nanoprobes, immediately (0 h) and after 24 h incubation of the magnetic nanoprobes in the corresponding buffered solutions at 37 °C. First, we observed that the T_1 relaxation rate ($1/T_1$) of the IO-PAA-Gd-DTPA nanoprobe (0 h, Figure 1A) was similar to that of the control IO-PAA nanoprobe (0 h, Supporting Information, Figure S2A) at all pH values (pH 4.0−7.4). This observation seems to indicate that in the IO-PAA-Gd-DTPA nanoprobe the $1/T_1$ of Gd-DTPA was quenched upon encapsulation in the polymeric coating of IO-PAA. In contrast, we observed a greater increase in $1/T_1$ of the IO-PAA-Gd-DTPA nanoprobe when incubated in acidic [pH = 4.0 (▼), 5.0 (▲), and 6.0 (●)] buffered solution after 24 h (Figure 1B). However, no changes in $1/T_1$ were observed either for IO-PAA-Gd-DTPA when incubated at physiological pH over the same 24 h time period (pH = 7.4, ■, Figure 1B) or for equivalent concentrations of control IO-PAA across the same pH values (pH 4.0 to 7.4) after 24 h of incubation (Supporting Information, Figure S2B). These results suggest that the composite IO-PAA-Gd-DTPA nanoprobe gets activated, resulting in high $\Delta 1/T_1$ numbers (Figure 1C) within 24 h of incubation in the acidic buffered solutions in contrast to values obtained with the control IO-PAA probe (Supporting Information, Figure S2C). In another set of experiments, minimal changes in T_2 relaxation rate ($\Delta 1/T_2$) were observed for both the composite IO-PAA-Gd-DTPA nanoprobe (Figure 1D−F) and control IO-PAA nanoprobe

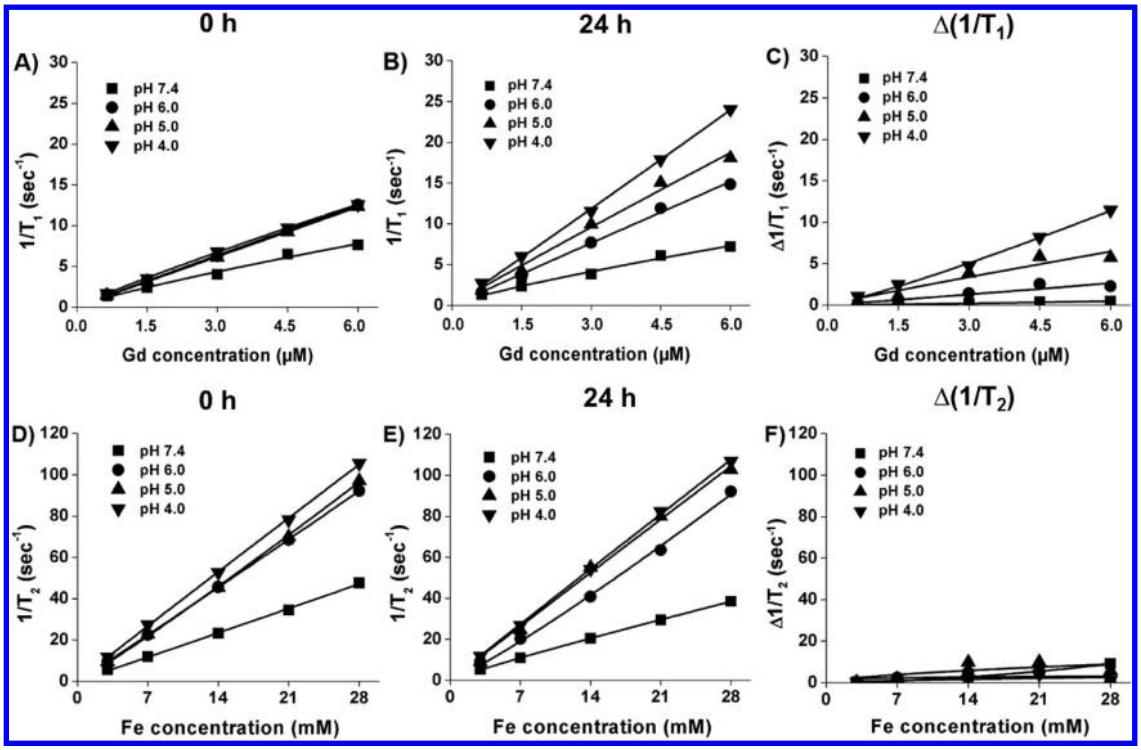

Figure 1. Assessment of magnetic relaxations of activatable magnetic nanoprobe IO-PAA-Gd-DTPA using a benchtop magnetic relaxometer (Bruker's Minispec, B = 0.47 T). Inverse spin−lattice ($1/T_1$) and spin−spin ($1/T_2$) magnetic relaxation times were measured before and after 24 h of incubation in different PBS solutions (pH 4.0−7.4, 37 °C) and at different nanoprobe concentrations. (A) Initial $1/T_1$ measurements right after the addition of PBS solutions, (B) $1/T_1$ measurements after 24 h of incubation, (C) differential $1/T_1$ values prior to and after incubation. (D) Initial $1/T_2$ measurements right after the addition of PBS solutions, (E) $1/T_2$ measurements after 24 h of incubation, (F) differential $1/T_2$ values prior to and after incubation (means ± SE; SE were within 1−4%, which are too small to be depicted).

(Supporting Information, Figure S2D−F) when incubated for 24 h in buffered solutions (pH 4.0 to 7.4). These results indicated that the T_2 of IO-PAA-Gd-DTPA probe was not quenched upon encapsulation of the Gd-DTPA complex, as hypothesized. Taken together, the above results suggest that the inverse spin−lattice magnetic relaxation ($1/T_1$) of our composite IO-PAA-Gd-DTPA nanoprobes got activated when exposed to acidic environments and could be of potential use as an activatable NMR/MRI imaging agent for the detection of tumors, upon internalization and localization of the nanoprobes within lysosomes.

pH-Dependent Studies of a Gd-DTPA Cerium Oxide Nanocomposite as Control Studies. To confirm that the superparamagnetic nature of the iron oxide core is responsible for quenching the magnetic relaxation of the Gd-DTPA, we synthesized a PAA-coated cerium oxide nanoparticle encapsulating Gd-DTPA (NC-PAA-Gd-DTPA). In this design, we selected a nonmagnetic metal oxide core composed of cerium oxide (nanoceria, NC) to replace the magnetic iron oxide core during our synthesis protocol. We reasoned that incorporation of Gd-DTPA within the polymeric coating of a nonmagnetic nanoparticle, such as cerium oxide, will not result in T_1 quenching or activation upon incubation in acidic media. The NC-PAA-Gd-DTPA nanoprobes were synthesized following a procedure similar to the one used to synthesize the IO-PAA-Gd-DTPA nanoprobe. Briefly, to a PAA solution in water, Gd-DTPA was added and mixed thoroughly before addition to a solution of cerium nitrate in ammonium hydroxide solutions. The synthesized NC-PAA-Gd-DTPA composite nanoprobe was purified using the SpectrumLab's Krosflo filtration system. DLS and ICP-MS of the nanoprobe aqueous suspension indicated the presence of 88 ± 1 nm nanoparticles with a Gd concentration of 0.315 mg/mL (Supporting Information, Scheme S1). These values were similar to those obtained for the IO-PAA-Gd-DTPA nanoprobes, suggesting that the size, polymer coating thickness, and amount of encapsulated Gd were similar in both preparations. Magnetic relaxation values of the aqueous nanoparticle suspension revealed an $r_1 = 34.3 \pm 2.1$ mM^{-1} s^{-1} and $r_2 = 60 \pm 5.2$ mM^{-1} s^{-1} (based on Gd concentration), further confirming the successful encapsulation of Gd in the nanoparticle's polymeric core. The magnetic relaxation rates $1/T_1$ and $1/T_2$ of the NC-PAA-Gd-DTPA nanoprobes indicated no change in $\Delta 1/T_1$ (Figure 2C) before (0 h, Figure 2A) or after 24 h incubation (Figure 2B) in either physiological (pH 7.4) or acidic (pH 4.0) buffered solutions, indicating no magnetic relaxation activation at acidic pH. Similarly, no changes in T_2 ($\Delta 1/T_2$, Figure 2D−F) were recorded for the NC-PAA-Gd-DTPA nanoprobes, and as expected, no changes in magnetic relaxation rates ($1/T_1$ and $1/T_2$) were

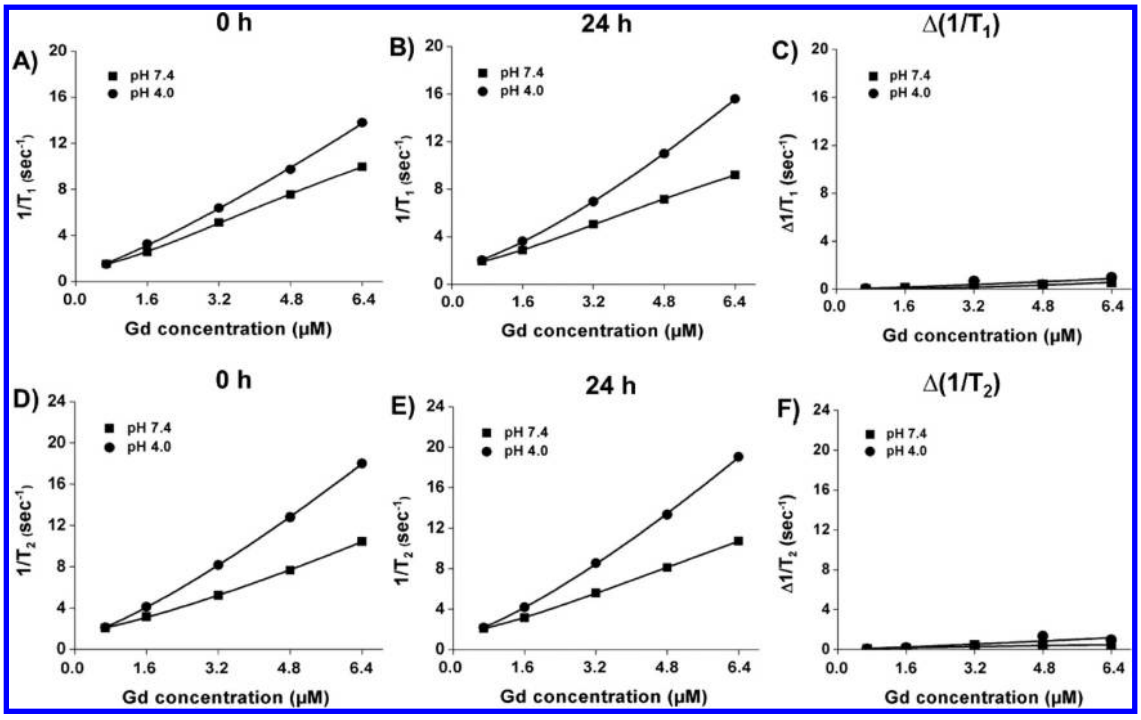

Figure 2. Assessment of magnetic relaxations of composite nanoceria NC-PAA-Gd-DTPA using a benchtop magnetic relaxometer (Bruker's Minispec, B = 0.47 T). Inverse spin−lattice ($1/T_1$) and spin−spin ($1/T_2$) magnetic relaxation times were measured before and after 24 h of incubation in different PBS solutions (pH 4.0 and 7.4, 37 °C) and at different nanoprobe concentrations. (A) Initial $1/T_1$ measurements right after the addition of PBS solutions, (B) $1/T_1$ measurements after 24 h of incubation, and (C) differential $1/T_1$ values prior to and after incubation. (D) Initial $1/T_2$ measurements right after the addition of PBS solutions, (E) $1/T_2$ measurements after 24 h of incubation, and (F) differential $1/T_2$ values prior to and after incubation (means ± SE; SE were within 1−4%, which are too small to be depicted).

observed in the case of nonmagnetic nanoceria control probe NC-PAA[61,62] (Supporting Information, Figure S3). Taken together, the above results suggest that the observed quenching of the Gd-DTPA T_1 relaxation rate ($1/T_1$) only occurred when the Gd-DTPA was encapsulated in close proximity to a superparamagnetic core (iron oxide) and not when encapsulated within the polymeric coating of a nonmagnetic core. These data also suggest that the observed quenching is not due to immobilization of the Gd-DTPA within a polymer matrix surrounding a nonmagnetic core (cerium oxide). In another set of experiments, no significant pH-dependent activation was observed when an iron oxide nanocomposite containing Ca-DTPA instead of Gd-DTPA was used, further indicating that the release of the paramagnetic Gd-chelate is responsible for the observed activation in acidic pH (Supporting Information, Figure S4). Taking together, these results indicate that the observed pH-dependent T_1 activation observed with our IO-PAA-Gd-DTPA nanocomposite is due to quenching of the T_1 relaxativity of the Gd-DPTA chelate when in close proximity to the iron oxide core and subsequent activation upon release from the nanoparticle's polymeric coating.

Magnetic Relaxations of the Gd-DTPA Surface Conjugating Magnetic Nanoprobes. In our hypothesis, we stated that the close proximity of Gd (a weak paramagnetic ion) within the polymeric matrix of iron oxide nanoparticles (a strong superparamagnetic nanocrystal) affects the T_1 relaxation of Gd. If our hypothesis is correct, conjugation of a Gd-DTPA directly on the nanoparticle's surface will not result in quenching of the T_1 values. In this case, the Gd-DTPA will be further away from the iron oxide core and its T_1 relaxation will be less affected by the strong magnetic susceptibility of the magnetic core. To further test this hypothesis, we then synthesized a IO-PAA-Gd-DTPA magnetic nanoprobe where the Gd-DTPA was conjugated directly on the IO-PAA surface carboxylic acid groups (Supporting Information, Scheme S2). Briefly, IO-PAA was first conjugated with ethylenediamine using the water-soluble carbodiimide chemistry, as previously described.[22] The resulting aminated IO-PAA was then conjugated with Gd(III)-chelated 2-(4-isothiocyanatobenzyl)diethylenetriaminepentaacetic acid (*p*-SCN-Bn-Gd-DTPA) in basic PBS buffer (pH 8.4). The conjugated magnetic nanoprobe was purified using small magnetic columns (Miltenyi Biotech) and washed with PBS (pH 7.4), prior to characterizations and magnetic relaxation measurements. The successful conjugation of the functional Gd-DTPA complex was confirmed by performing ICP-MS experiments, and the resulting Gd concentration was found to be 0.201 mg/mL. The amount of Fe in the preparation was determined as 2.0 mg Fe/mL, for a 0.04:1 Gd/Fe molar ratio. The magnetic relaxation values of the conjugated nanoprobe were $r_1 = 63.4 \pm 1.5\ mM^{-1}\ s^{-1}$ and $r_2 = 92.1 \pm 3.8\ mM^{-1}\ s^{-1}$ (based on Gd concentration), and r_1 = 49.9 ± 1.3 $mM^{-1}\ s^{-1}$ and r_2 = 243 ± 3 $mM^{-1}\ s^{-1}$

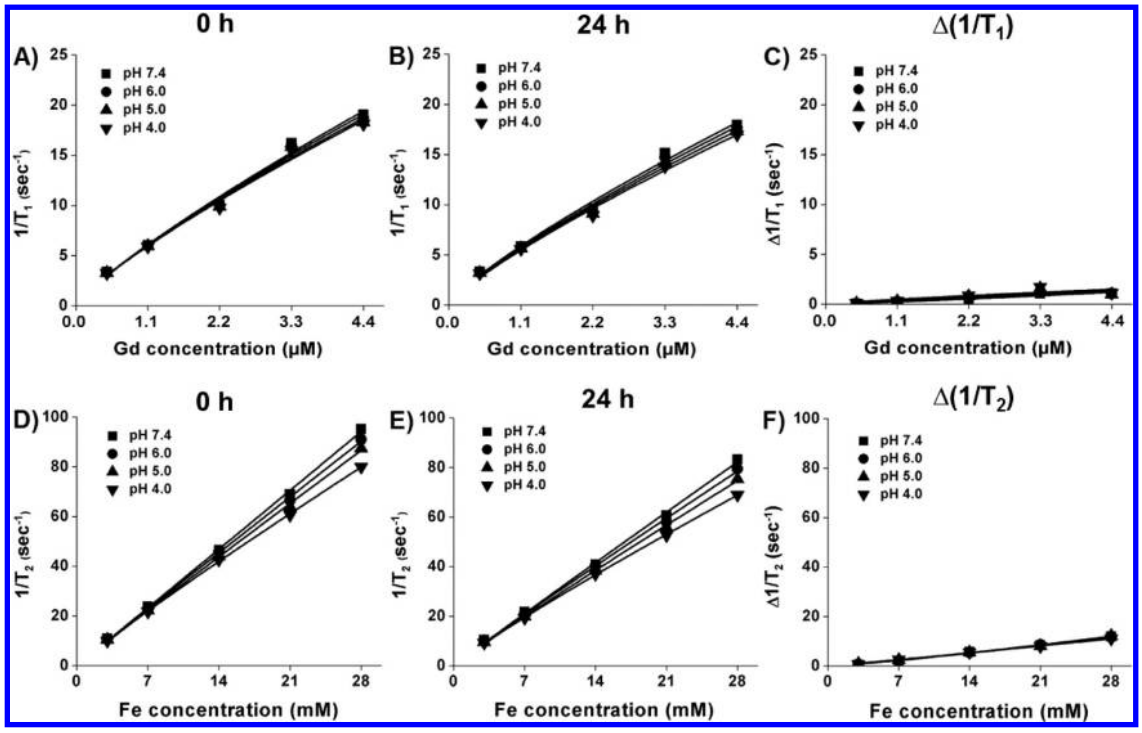

Figure 3. Assessment of magnetic relaxations of Gd-DTPA surface conjugating IO-PAA magnetic nanoprobes, using a benchtop magnetic relaxometer (Bruker's Minispec, B = 0.47 T). Inverse spin−lattice ($1/T_1$) and spin−spin ($1/T_2$) magnetic relaxation times were measured before and after 24 h of incubation in different PBS solutions (pH 4.0−7.4, 37 °C) and at different nanoprobe concentrations. (A) Initial $1/T_1$ measurements right after the addition of PBS solutions, (B) $1/T_1$ measurements after 24 h of incubation, and (C) differential $1/T_1$ values prior to and after incubation. (D) Initial $1/T_2$ measurements right after the addition of PBS solutions, (E) $1/T_2$ measurements after 24 h of incubation, and (F) differential $1/T_2$ values prior to and after incubation (means ± SE; SE were within 1−4%, which are too small to be depicted).

(based on Fe concentration). The T_1 and T_2 relaxation rates ($1/T_1$ and $1/T_2$) of the nanoprobe were measured in a similar fashion as described earlier and results compared to those of the control IO-PAA nanoprobe. Results showed no change in $\Delta 1/T_1$ (Figure 3C) before (0 h, Figure 3A) or after (24 h, Figure 3B) incubating in various buffered solutions and were found to be similar to that of the control IO-PAA probe with no magnetic activation (Supporting Information, Figure S2). Similarly, no changes in spin−spin relaxations ($\Delta 1/T_2$, Figure 3D−F) were observed after the 24 h of treatment. Overall, the above results indicate the encapsulation of the Gd-DTPA within the polymeric coating and close proximity to the iron oxide core responsible for the Gd relaxation quenching, which was then activated upon release.

Meanwhile, the r_1 and r_2 relaxation values based on Gd concentrations of the IO-PAA-Gd-DTPA nanoprobes indicate a significant pH-dependent increase in the r_1 of the nanoprobes when the Gd is encapsulated within the polymeric coating of the iron oxide nanoparticles (Table 1). Results show that, by decreasing the pH of the solution to a mildly acidic condition (pH 6.0), a significant percent increase of 44% in the Gd-based r_1 is observed. This value contrasts with a small increase of 5% observed when the Gd is conjugated on the nanoparticle surface, further indicating that indeed encapsulation within the nanoparticle's polymeric matrix is essential for the observed T_1 activation. The observed increase in r_1 is larger at higher pH, observing a 68% increasing at pH 5.0, the typical pH within lysosomes. Even though pH-dependent percent changes in r_2 are also observed in the Gd-encapsulated nanocomposite, they are not as large as the values obtained with r_1. Taken together, these results confirm the T_1 activation of the IO-PAA-Gd-DTPA nanoprobes upon decreases in pH, particularly within the range (pH 6−5) observed within lysosomes.

MRI-Based T_1-Weighted Activation of the Composite IO-PAA-Gd-DTPA Nanoprobe. Next, we investigated if the observed pH-dependent increases in r_1 of the IO-PAA-Gd-DTPA nanoprobe results in increases in the T_1-weighted signal by MRI, leading to an increase in the brightness of the image. For these experiments, the T_1- and T_2-weighted MR images (MRI, B = 4.7 T) of nanoprobe solutions at pH 5.0 were acquired immediately (Figure 4A1) and after a 24 h incubation (Figure 4A2) in the pH 5.0 buffer. An increase in the T_1-weighted MR signals was observed as the concentration of the activatable IO-PAA-Gd-DTPA nanoprobes increased (from 0.06 to 2.4 μM of Gd), resulting in an increase in the signal of the corresponding MR images (Figure 4A2). The observed signal increase after a 24 h incubation in the pH 5.0 buffer corresponded to an increase in the ($1/T_1$) relaxation rate (▲, Figure 4C). As expected, a minimal increase in T_2-weighted MR

TABLE 1. Magnetic Relaxation Values at 0.47 T of the Nanocomposite Based on Gd Concentrations at Different pH

nanoprobe	pH	r_1 (mM^{-1} s^{-1})	r_2 (mM^{-1} s^{-1})	% change r_1	% change r_2
IO-PAA-Gd-DTPA (encapsulated) [Gd] = 0.289 mg/mL	7.4	50.2 ± 1.8	87.3 ± 2.4		
	6.0	72.5 ± 1.3	98.2 ± 3.2	44	12
	5.0	84.3 ± 1.2	111.6 ± 2.8	68	28
	4.0	97.0 ± 2.5	118.5 ± 3.4	93	38
IO-PAA-Gd-DTPA (surface) [Gd] = 0.201 mg/mL	7.4	63.4 ± 1.5	92.1 ± 3.8		
	6.0	66.3 ± 2.2	95.2 ± 1.2	5	3
	5.0	68.1 ± 1.4	97.4 ± 2.1	7	6
	4.0	69.3 ± 1.3	98.5 ± 1.8	9	7

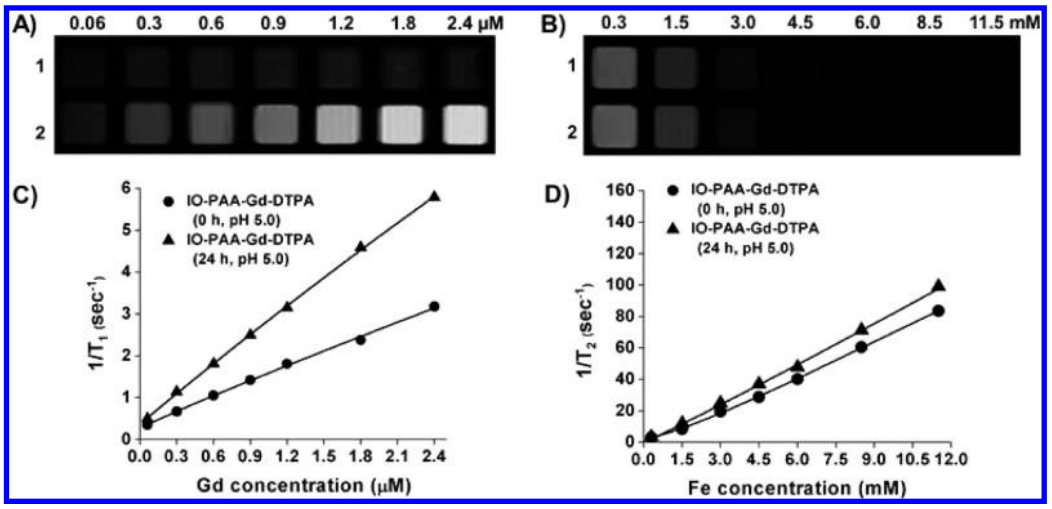

Figure 4. Magnetic resonance imaging (MRI) studies measuring the magnetic activations (T_1 and T_2 map) of our activatable magnetic IO-PAA-Gd-DTPA nanoprobes in PBS at pH 5.0. (A) T_1-weighted MRI images of increasing Gd concentrations (0.06−2.4 μM) of IO-PAA-Gd-DTPA nanoprobes prior to (1) and after 24 h of incubation (2) at 37 °C. (B) T_2-weighted MRI images of increasing Fe concentrations (0.3−11.5 mM) of IO-PAA-Gd-DTPA nanoprobes prior to (1) and after 24 h of incubation (2) at 37 °C. (C) Corresponding $1/T_1$ relaxation rates prior to (●) and after (▲) 24 h of incubation. (D) Corresponding $1/T_2$ relaxation rate prior to (●) and after (▲) 24 h of incubation (means ± SE; SE were within 1−4%, which are too small to be depicted).

signals (T_2 map, Figure 4B) or corresponding inverse spin−spin magnetic relaxations ($1/T_2$, Figure 4D) was observed from the IO-PAA-Gd-DTPA nanoprobes due to the absence of any T_2 activation. However, in this case, the MR signals were found to be decreased since the iron concentrations increased with the rising nanoprobe concentrations. The calculated r_1 and r_2 values at 4.7 T for the IO-PAA-Gd-DTPA nanoprobe before and after a 24 h incubation at pH 5.0 also show an increase in r_1 values (24.8 ± 1.2 *vs* 45.2 ± 1.9 mM^{-1} s^{-1}) for a percent increase in r_1 of 87%. Meanwhile, a modest increase in r_2 was observed (75.4 ± 2.3 *vs* 91.5 ± 3.1 mM^{-1} s^{-1}) for a percent increase of only 21%. In another set of experiments, no change in the MR signals (both T_1 and T_2 map) or corresponding magnetic relaxations were observed due to the absence of any magnetic activation from our control IO-PAA probe (Supporting Information, Figure S5). Taken together, the above results confirm that our activatable IO-PAA-Gd-DTPA nanoprobes get activated at acidic pH, and activation was indicated by the increase in the T_1-weighted MRI signal. These results also suggest the potential diagnostic applications of our novel NMR/MRI activatable composite iron oxide nanoprobes.

***In Vitro* Activation of the Composite IO-PAA-Gd-DTPA Nanoprobe.** To evaluate the potential biomedical applications of the activatable IO-PAA-Gd-DTPA nanoprobes, we assessed their magnetic activations using cultured cells. We hypothesized that, upon receptor-mediated endocytosis, the nanoparticles will localize in acidic lysosomes, therefore becoming activated as the encapsulated Gd-DTPA complex gets released at lower pH. For these experiments, the magnetic nanoprobes were functionalized with folic acid, following published protocols,[22,63] in order to assess their targeted imaging capabilities toward folate receptor (FR)-expressing cancer cells. We hypothesized that, upon internalization into FR-expressing cancer cells, T_1 activation of the composite IO-PAA-Gd-DTPA-Fol nanoprobe would be triggered by the lysosomal acidic environment (pH 5.0), resulting in *in vitro* activation of the MRI signals. In these experiments, we used a FR-positive human cervical carcinoma cell line (HeLa cells, 10 000 cells/well), and as negative control, we used H9c2 cardiomyocyte (10 000 cells/well) that do not express FR. Cells

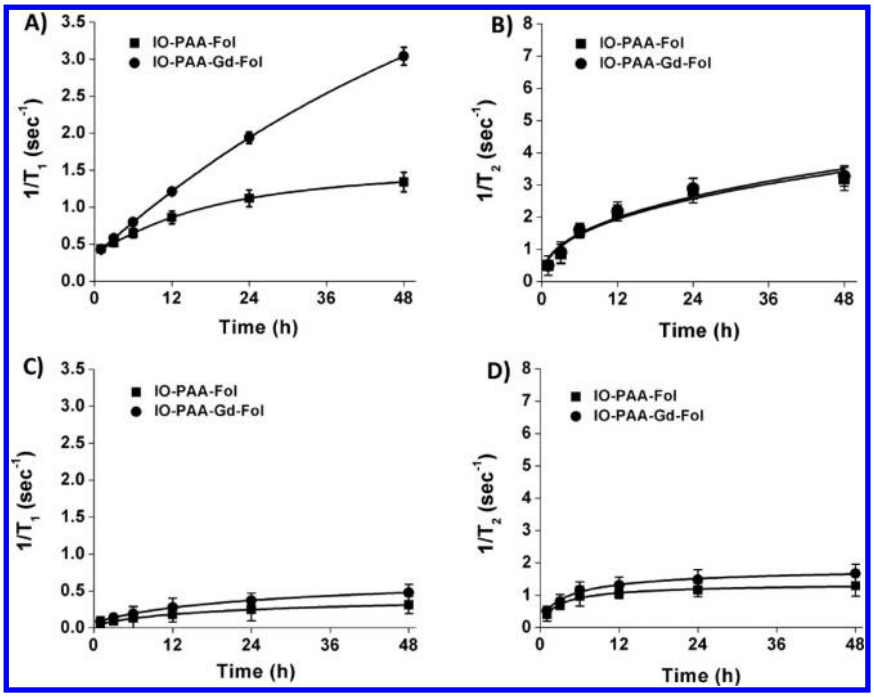

Figure 5. Intracellular magnetic activations of our folate-decorated activatable IO-PAA-Gd-DTPA-Fol nanoprobe (●, 100 μL, 28 mM) and the control IO-PAA-Fol nanoprobe (■, 100 μL, 28 mM) using FR-expressing HeLa cells (A,B) and FR-negative H9c2 cells (C,D). Significant activation in inverse spin−lattice magnetic relaxations ($1/T_1$) was observed from HeLa cells incubated with the activatable IO-PAA-Gd-DTPA-Fol nanoprobes (●,A). As expected, no significant changes in $1/T_2$ were observed from HeLa cells due to absence of any T_2 activations (B). Neither $1/T_1$ (C) nor $1/T_2$ (D) activations were observed from H9c2 cells due to lack of any receptor-mediated internalizations.

were incubated with the nanoprobes (100 μL, 28 mM) at different time points, trypsinized, centrifuged, and resuspended in PBS (pH 7.4) before measuring T_1 and T_2 of the nanoparticle cell suspension. As hypothesized, compared to the control IO-PAA-Fol nanoprobes, significant activation in inverse spin−lattice magnetic relaxations ($1/T_1$) was observed in HeLa cells incubated with the activatable IO-PAA-Gd-DTPA-Fol nanoprobes (●, Figure 5A). No significant changes in $1/T_2$ were observed from HeLa cells incubated with either of the probes (Figure 5B). These results further supported the *in vitro* activatable MR imaging capability of the composite nanoprobes, whereas the control probe's (■, IO-PAA-Fol) magnetic relaxation remained unchanged after the FR-mediated internalizations. In contrast, no significant changes in magnetic relaxations (both $1/T_1$ and $1/T_2$) were observed from H9c2 cells (FR-negative) incubated with either one of the nanoprobes, suggesting the lack of any receptor-mediated internalizations of our magnetic nanoprobes (Figure 5C,D). Furthermore, control experiments using HeLa cells preincubated with excess folic acid (0.2 mg/mL) in the culturing media resulted in abrogation of the pH-dependent $1/T_1$ activation (Supporting Information, Figure S6). Taken together, our results confirm that the FR-mediated internalizations and lysosomal acidic pH-assisted release of the encapsulating Gd-DTPA complex were responsible for the enhanced MR signal from our composite IO-PAA-Gd-DTPA-Fol nanoprobe. These results also indicate that the activatable MR imaging capability of our composite nanoprobe could potentially be useful in the detection and treatment of cancer in clinical settings.

pH-Dependent Dual Release of the Gd-DTPA Complex and Taxol. Previously, we have reported the encapsulation and release of a cytotoxic drug (Taxol) from the polymeric coating of iron oxide nanoparticles as a theranostic nanoagent for the potential treatment of cancer.[22] We then hypothesized whether we could encapsulate both Taxol and Gd-DTPA within the same nanoparticle, creating a dual therapeutic and activatable magnetic nanoprobe. The IO-PAA-Gd-DTPA nanoprobes were then used to encapsulate Taxol as previously described using the solvent diffusion method.[22,63] Briefly, to a suspension of IO-PAA-Gd-DTPA nanoprobes (2.5 mL, 28 mmol) in PBS, the dimethyl sulfoxide (DMSO) solution of Taxol (10 μL, 0.5 μg/μL) was added dropwise at room temperature. The resulting purified IO-PAA-Gd-DTPA-Taxol nanoparticles were characterized by measuring their size using DLS (D = 84 ± 2 nm), taxol encapsulation efficiency (EE) = 52 ± 2.4% using HPLC (λ_{abs} = 227 nm), and calculating the Gd concentration (0.215 mg/mL) by performing ICP-MS experiments. To evaluate the dual release of Taxol and Gd, the IO-PAA-Gd-DTPA-Taxol nanoprobes were incubated in a pH 5.0 PBS solution, and the rate of release of the drug and Gd was assessed using a dynamic dialysis technique. Briefly,

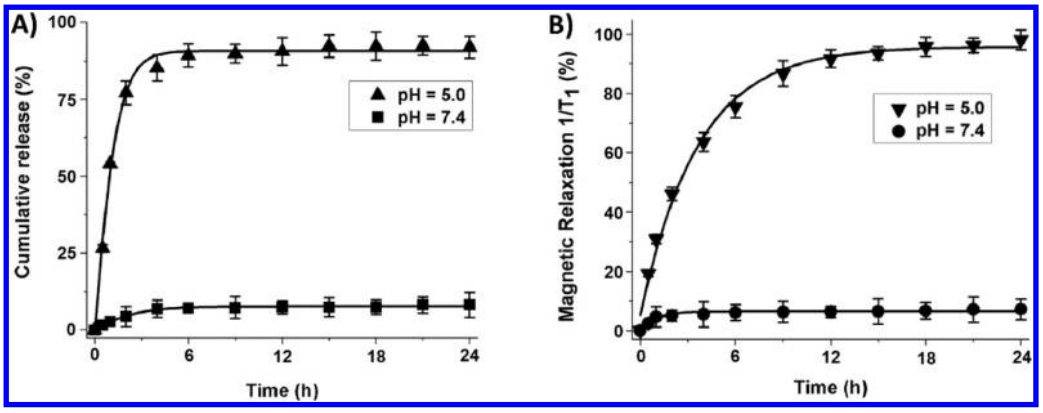

Figure 6. Rate of release of Taxol and Gd-DTPA at 37 °C. (A) HPLC experiment (λ_{abs} = 227 nm) indicated the time-dependent release of Taxol from the activatable IO-PAA-Gd-DTPA nanoprobes (50 μL, 28 mM) when incubated at pH 5.0 (▲) solution. No significant release of Taxol was observed (■) when incubated in PBS at pH 7.4. (B) Observed increase rate of Taxol release was accompanied by a gradual increase in the inverse spin−lattice magnetic relaxation ($1/T_1$) recorded using magnetic relaxometer (▼, B = 0.47 T, pH 5.0). As expected, nominal increase in the inverse spin−lattice magnetic relaxation (●, $1/T_1$) was observed when incubated in PBS at pH 7.4.

the IO-PAA-Gd-DTPA-Taxol nanoprobes (50 μL, 28 mM) were taken in a small dialysis cup (MWCO 6−8 kDa) and incubated in PBS (pH 5.0) solution at 37 °C. The rate of release of Taxol and Gd was monitored by collecting aliquots from the outside reservoir buffer and measuring the amount of released taxol *via* HPLC experiment (λ_{abs} = 227 nm) and Gd by measuring the increase in T_1 relaxation rate with time. Results showed a time-dependent increase in the amount of Taxol (▲, Figure 6A) and Gd-DTPA (▼, Figure 6B) released upon incubation at pH 5.0. These results suggest that indeed the acid-mediated degradation and/or swelling of the PAA coatings results in the simultaneous release of both Taxol and Gd. Interestingly, a slower rate of Gd-DTPA release from the nanoprobe is observed in contrast to Taxol, and this could be due to a possible higher extent of hydrogen bonding between Gd-DTPA and the carboxylic groups within the polymeric coating internal cavities surrounding the iron oxide core. In contrast, when similar experiments were performed at physiological pH (PBS, pH 7.4, 37 °C), no significant release of Taxol (■, Figure 6A) or Gd was observed (●, Figure 6B). Similarly, no significant release of Taxol or increase in magnetic relaxations ($1/T_1$) was observed when the IO-PAA-Gd-DTPA-Taxol nanoprobe was incubated in serum at 37 °C (Supporting Information, Figure S7). These findings indicate that the IO-PAA-Gd-DTPA-Taxol nanoprobe is stable at neutral pH and physiological conditions, only releasing its cargo (Taxol and Gd) in an acidic environment.

***In Vitro* Cytotoxicity of Taxol-Encapsulating Activatable IO-PAA-Gd-DTPA Nanoprobes.** Finally, we examined the differential *in vitro* cytotoxicity of the functionalized magnetic nanoprobes (35 μL, 28 mM in PBS, pH 7.4) using FR-expressing human cervical cancer cells (HeLa, 2500 cells/well) and FR-negative cardiomyocyte cell lines (H9c2, 2500 cells/well). Results confirmed a time-dependent decrease in the number of viable HeLa cells when incubated with folate-decorated IO-PAA-Gd-DTPA-Taxol nanoprobes **5** (Figure 7A), showing more than 90% reduction in cell viability after 24 h of incubation. However, the folate-decorated IO-PAA-Gd-DTPA nanoprobes showed nominal toxicity (**4**) and comparable with the IO-PAA-Fol (**1**) lacking the Gd-DTPA complex, as published earlier.[22] As expected, nominal cytotoxicity was observed when HeLa cells were incubated with the IO-PAA-Gd-DTPA (**2**) and IO-PAA-Gd-DTPA-Taxol (**3**), due to the absence of any receptor-mediated internalizations. These results suggest that the cytotoxicity of the nanoprobes was not affected by the encapsulation of Gd due to the presence of PAA polymer coatings. In addition, no significant reduction in cell viability was observed when H9c2 cells, which do not overexpress FR, were incubated with all of the functional magnetic nanoprobes (Figure 7B), suggesting biocompatibility and potential applications of our nanoprobes for the targeted imaging and treatment of cancers. Taken together, the above results suggest that our folate-decorated activatable IONP-PAA-Gd-DTPA-Taxol nanoprobes can potentially be used to detect tumors using MR imaging, while targeting and delivering a chemotherapeutic agent (Taxol) *via* folate receptors.

CONCLUSION

In summary, we report an activatable Gd-DTPA-encapsulating iron oxide NMR/MRI nanoprobe, with quenched longitudinal (spin−lattice) magnetic relaxation (T_1) of the encapsulated Gd-DTPA (low $1/T_1$) by the iron oxide nanoparticles. In our design, the T_1 relaxation of the Gd-DTPA complex becomes activated (dequenched), resulting in higher $1/T_1$ values and enhanced T_1-weighted MRI contrast, upon acid-mediated degradation and release of the T_1 agent. Our results clearly indicated that the magnetic relaxation of the Gd-DTPA chelate (T_1 agent) is quenched as a result of such encapsulation, whereas the transverse (spin−spin) magnetic relaxation (T_2) of iron oxide was

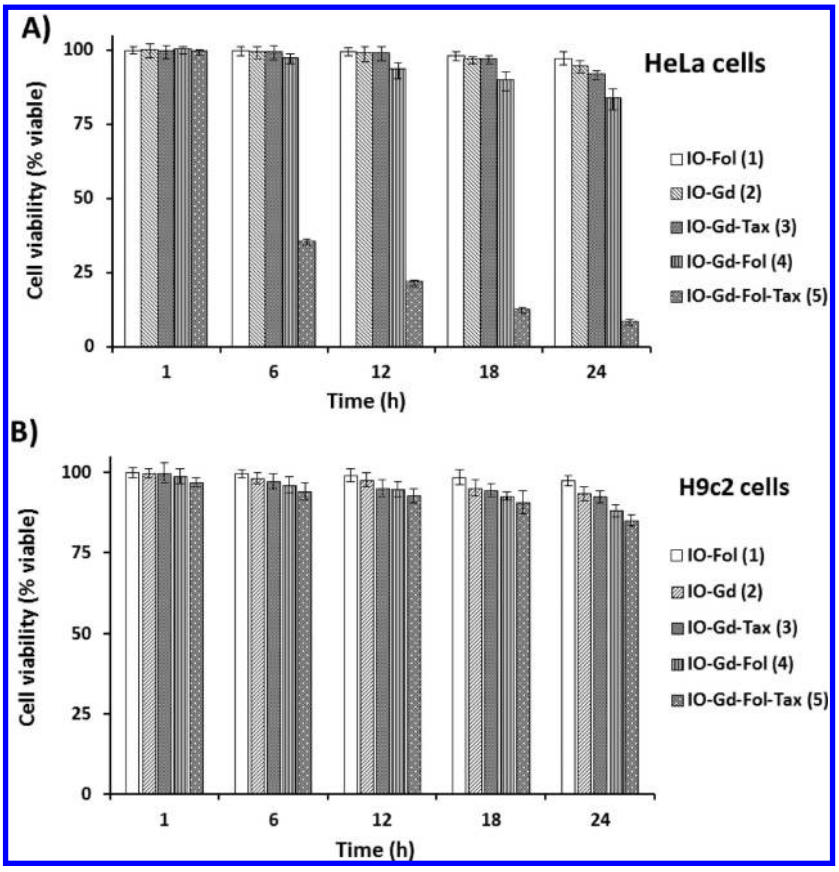

Figure 7. ***In vitro*** **cytotoxicity of Taxol-encapsulating activatable IO-PAA-Gd-DTPA nanoprobes. Time-dependent** ***in vitro*** **MTT assays for the determination of cytotoxicity of the functional magnetic nanoprobes (1−5, 35 μL, 28 mM in PBS, pH 7.4). HeLa cells (A) and H9c2 cells (B) treated with the functional magnetic nanoprobes. Folate-conjugated (1), Gd-DTPA-encapsulating (2), Gd-DTPA, and taxol-encapsulating (3) magnetic nanoprobes showed biocompatibility with nominal toxicity in both the cell lines. The Gd-DTPA-encapsulating folate-conjugated magnetic nanoprobes (4) showed more than 15% reduction in cell viability, whereas Gd-DTPA- and Taxol-encapsulating folate-conjugated magnetic nanoprobes (5) showed more than 90% reduction in cell viability when treated with HeLa cells (A) and not with H9c2 cells (B), confirming the folate-receptor-mediated internalizations and ability for targeted therapy. Average values of four measurements are depicted ±standard errors.**

minimally affected. Our results also demonstrated that the folate-receptor-mediated internalization and the subsequent lysosomal localization induced an intracellular release of Gd-DTPA complex, resulting in an enhanced $1/T_1$ signal. In addition, when a Taxol-encapsulating activatable magnetic nanoprobe was used, the intracellular drug's release was monitored by the observed changes in $1/T_1$. The presence of folate on the activatable magnetic nanoprobe guarantees a selective activation and release of the drug only in folate-receptor-positive cells, minimizing toxicity to healthy cells. In contrast, no T_1 activation is observed in the Gd-DTPA surface-conjugated IONPs or Gd-DTPA-encapsulating nonmagnetic NC-PAA, confirming that quenching was due to the close residence of the Gd-DTPA to the superparamagnetic iron oxide (IO) core and not due to the presence of any nonmagnetic metallic core (cerium oxide) or polymeric (PAA) coatings. Overall, the pH dependence and targeted activation upon cellular internalization of our designed IO-PAA-Gd-DTPA nanoprobe are important attributes of this novel platform technology that can be further developed into others MR-activatable and theranostic nanoprobes.

MATERIALS AND METHODS

Materials. Iron salts, including ferrous(II) chloride tetrahydrate ($FeCl_2 \cdot 4H_2O$) and ferric(III) chloride hexahydrate ($FeCl_3 \cdot 6H_2O$), gadolinium(III) chloride hexahydrate ($GdCl_3 \cdot 6H_2O$), cerium(III) nitrate hexahydrate ($CeNO_3 \cdot 6H_2O$), diethylenetriaminepentaacetic acid (DTPA), ammonium hydroxide, hydrochloric acid, sodium hydroxide, chloropropryl amine, sodium azide, copper(I) iodide, ethylenediamine (EDA), folic acid, *N*,*N*-dimethylformamide (DMF), dimethyl sulfoxide (DMSO), 3-(4,5-dimethylthiazol-2-yl)-2, 5-diphenyltetrazolium bromide (MTT), *N*-hydroxysuccinimide (NHS), 2-(*N*-morpholino) ethanesulfonic acid (MES), poly(acrylic acid) (PAA) and other chemicals, were purchased from Sigma-Aldrich. 2-(4-Isothiocyanatobenzyl)diethylenetriaminepentaacetic acid [*p*-SCN-Bn-DTPA] was purchased from Macrocyclics. EDC [1-ethyl-3-(3-dimethylaminopropyl)carbodiimide hydrochloride] was obtained from Pierce Biotechnology. The human cervical carcinoma (HeLa) and cardiomyocyte (H9c2) cell lines were obtained from ATCC. Magnetic columns (LS Column) were

purchased from Miltenyi Biotech for the purification of magnetic nanoprobes using QuadroMACS separators. Dialysis membranes were obtained from Spectrum Laboratories. Nitrogen-purged DI water was used in all syntheses.

Synthesis of the Gd-DTPA Complexes. Chelation of the rare-earth element gadolinium (Gd) with diethylenetriaminepentaacetic acid (DTPA) or with functional DTPA, *p*-SCN-Bn-DTPA [2-(4-isothiocyanatobenzyl)diethylenetriaminepentaacetic acid], results in a strongly paramagnetic, stable complex that is well-tolerated in animals. These complexes were synthesized following the reported literature method.[64,65] Briefly, a solution of $GdCl_3 \cdot 6H_2O$ (4.49 g, 0.0121 mol) in H_2O (10 mL) was added dropwise to a solution of DTPA (5.0 g, 0.0127 mol) or *p*-SCN-Bn-DTPA (0.0127 mol) in H_2O (30 mL) containing 2 N NaOH (5.0 mL) solution. The pH of the final reaction mixture was maintained at 6.8 by constant addition of 2 N NaOH solution. The reaction was continued at 80 °C for 12 h before concentrated to 20 mL. The observed white crystals were dissolved in a minimum amount of water before precipitating in ethanol. The precipitate was filtered and dried under vacuum to obtain the Gd(III) complex as a white solid (yield: 86%).

Synthesis of the Gd-DTPA-Encapsulating Composite Iron Oxide Nanoprobes (IO-PAA-Gd-DTPA). For the synthesis of Gd-DTPA-encapsulating composite nanoprobe (IO-PAA-Gd-DTPA), we used a novel water-based, *in situ* encapsulation approach for the successful encapsulation of the Gd-DTPA complex. In this approach, three different solutions were prepared: an iron salt solution [0.61 g of $FeCl_3 \cdot 6H_2O$ and 0.32 g of $FeCl_2 \cdot 4H_2O$ in dilute HCl solution (100 μL of 12 N HCl in 2.0 mL H_2O)], an alkaline solution [1.8 mL of 30% NH_4OH solution in 15 mL of N_2 purged DI water], and a paramagnetic stabilizing solution [800 mg of PAA and 20 mg of Gd-DTPA complex in 5 mL of DI water]. To synthesize the composite IO-PAA-Gd-DTPA nanoprobe, the iron salt solution was added to the alkaline solution under vigorous stirring. The resulting dark suspension of iron oxide nanoparticles was stirred for 10 s before addition of the paramagnetic stabilizing solution and stirred for 1 h. The resulting suspension of the composite IO-PAA-Gd-DTPA nanoprobe was then centrifuged at 4000 rpm for 30 min to get rid of free poly(acrylic acid), Gd-DTPA complex, and other unreacted reagents. Finally, the composite IO-PAA-Gd-DTPA nanoprobe suspension was purified using magnetic columns and washed with phosphate buffer saline (pH 7.4) solution. The iron concentration and magnetic relaxation of the PAA-IONPs was determined as previously reported.[22] The successful coating of the IONPs with PAA was confirmed by the presence of a negative zeta-potential ($\zeta = -41$ mV) and the characteristic acid carbonyl band on the FT-IR spectroscopic analysis of the nanoparticles (Supporting Information, Figure S1).

Synthesis of the Theranostic Cargo-Encapsulating Composite Activatable Magnetic Nanoprobes. Taxol was encapsulated in the PAA polymer coating of the magnetic nanoprobe, following the previously reported solvent diffusion method.[22,66] Briefly, to a suspension of IO-PAA-Gd-DTPA nanoprobes (2.5 mL, 28 mmol) in PBS, a dimethyl sulfoxide (DMSO) solution of Taxol (10 μL, 0.5 μg/μL) was added dropwise at room temperature with continuous stirring at 1000 rpm. The Taxol-encapsulating nanoprobes (IO-PAA-Gd-DTPA-Taxol) were purified using a magnetic column (Miltenyi Biotech) and then dialyzed (using 6−8K MWCO dialysis bag) three times against deionized water and finally against phosphate buffered saline solution. The resulting IO-PAA-Gd-DTPA-Taxol nanoparticles were characterized by measuring their size using DLS ($D = 84 \pm 2$ nm), the Taxol encapsulation efficiency (EE) = 52 ± 2.4% using HPLC (λ_{abs} = 227 nm).

Synthesis of Folate-Decorated Magnetic Nanoprobes: Click Chemistry. To synthesize folate-decorated functional IO-PAA nanoprobes, the surface carboxylic acid groups of the nanoprobes were alkynated using propargylamine as a reagent, and the water-based carbodiimide chemistry was followed as previously reported.[22] The resulting alkynated IO-PAA nanoprobes were purified using magnetic columns. The highly specific "click" chemistry was used to conjugate an azide-functionalized folic acid with the purified alkynated IO-PAA, as described in the previously reported methods.[22,67] Briefly, the alkynated IO-PAA (4.0×10^{-3} mmol) in bicarbonate buffer (pH 8.5) was taken to an Eppendorf tube containing a catalytic amount of CuI (5.0×10^{-10} mmol) in 250 μL of bicarbonate buffer (pH 8.5) and vortexed. To the resulting solution, the azide-functionalized folic acid[22,63] (8.0×10^{-2} mmol) in DMSO was added and the reaction was incubated at room temperature for 12 h. The synthesized folate-decorated IO-PAA was purified using the magnetic column and finally washed using PBS solution (pH 7.4). The folate-decorate IO-PAA was stored in refrigerator for further characterization.

Synthesis of the Gd-DTPA-Encapsulating Composite Nanoceria (NC-PAA-Gd-DTPA). For the synthesis of Gd-DTPA-encapsulating composite nanoceria, we have modified our previously reported stepwise method[61,68] and followed the *in situ* encapsulation approach. In this approach, 1 M cerium(III) nitrate (2.17 g in 5.0 mL of water) solution was added to 30.0 mL of ammonium hydroxide solution (30% w/v) under continuous stirring at room temperature. Then, after 45 s of stirring, an aqueous mixture containing the PAA polymer and Gd-DTPA complex (800 mg of PAA and 20 mg of Gd-DTPA in 5 mL of water) was added and allowed to stir for 3 h at room temperature. The preparation was then centrifuged at 4000 rpm for two 30 min cycles to settle down any debris and large agglomerates. The supernatant solution was then purified from free PAA, Gd-DTPA complex, or other chemicals and concentrated using SpectrumLab's KrosFlo filtration system.

Synthesis of the Gd-DTPA Surface-Conjugating Magnetic Nanoprobes (IO-PAA-Gd-DTPA-Surface). The poly(acrylic acid)-coated iron oxide nanoparticles (IO-PAA) were synthesized using our previously reported alkaline precipitation method.[22] Briefly, an Fe^{3+}/Fe^{2+} solution in water was rapidly mixed with an ammonium hydroxide solution for 30 s, prior to addition of the PAA polymer solution in water. The synthesized IO-PAA was purified using magnetic columns to remove any unreacted reagents, and phosphate buffered saline (PBS, pH 7.4) was used as running solvent. To incorporate amine groups to the nanoparticles, ethylenediamine was used as an aminating agent and the water-based carbodiimide chemistry (using EDC and NHS reagents) was followed, as previously reported.[22,62] The successful amination of the IO-PAA nanoparticles was confirmed by measuring their overall positive surface charge ($\zeta = +15$ mV) using Malvern's Zetasizer. To synthesize the Gd-DTPA surface-conjugating IO-PAA nanoprobe, the aminated IO-PAA was reacted with the isothiocyanate group of the *p*-SCN-Bn-DTPA chelated with $GdCl_3 \cdot 6H_2O$ salt. In a typical reaction, the isothiocyanate functional Gd-DTPA chelate (*p*-SCN-Bn-Gd-DTPA, 25 mmol) was added to the aminated IO-PAA nanoprobe (1 mmol) in the presence of basic phosphate buffered saline (PBS, pH 8.4) and incubated overnight at room temperature. The resulting Gd-DTPA surface-conjugating IO-PAA nanoprobe was purified using small magnetic columns (Miltenyi Biotech) and washed with phosphate buffered saline (PBS, pH 7.4), prior to characterizations and magnetic relaxation measurements.

Measurement of the Hydrodynamic Diameter and Surface Zeta-Potential of the Functional IO-PAA. The size and dispersity of the synthesized composite IO-PAA was measured using dynamic light scattering (DLS) PDDLS/CoolBatch 40T instrument with Precision Deconvolve 32 software. The overall surface charges (zeta-potential) of this functional IO-PAA were measured using a Zetasizer Nano ZS from Malvern Instruments. These experiments were performed by placing 10 μL of the composite magnetic nanoprobes in 990 μL of distilled water. All measurements were performed in triplicate.

Measurement of Magnetic Relaxations. Magnetic relaxation measurements were conducted with a compact magnetic relaxometer (0.47 T mq20, Bruker), by taking composite magnetic nanoprobes with various concentrations. Magnetic resonance imaging (MRI) of the magnetic phantoms was achieved using the MRI/MRS facility utilizing a 4.7 T 33 cm bore magnet imaging/spectroscopy system (MSKCC, New York). All measurements were performed in triplicate.

HPLC Experiment. HPLC experiments were carried out using a PerkinElmer's Series 200 instrument to study drug release kinetics. In a typical experiment, upon addition of acidic PBS solution (pH 5.0) to the Taxol-encapsulating IO-PAA-Gd-DTPA

(50 μL, 28 mM), the rate of release of encapsulating Taxol was monitored in a timely manner at 37 °C using HPLC (λ_{abs} = 227 nm) chromatography.

Cell Cultures. The human cervical cancer (HeLa) and cardiomyocyte (H9c2) cells were obtained from ATCC and maintained in accordance to the supplier's protocols. Briefly, the cervical cancer cells were grown in a 5% FBS-containing DMEM medium supplemented with L-glutamine, streptomycin, amphotericin B, and sodium bicarbonate. The H9c2 cells were propagated in a 10% FBS-containing MEM medium containing penicillin, streptomycin, and bovine insulin (0.01 mg/mL). Cells were grown in a humidified incubator at 37 °C under 5% CO_2 atmosphere.

***In Vitro* Magnetic Activations of the Composite Nanoprobes.** The human cells (HeLa and H9c2, 10 000 cells/well) were incubated with the folate-decorated activatable IO-PAA-Gd-DTPA-Fol nanoprobe and the control IO-PAA-Fol nanoprobe (100 μL, 28 mM) at different incubation times. The cells were then trypsinized and centrifuged. The resulting cell pellet was suspended in phosphate buffer saline (PBS, pH 7.4), and magnetic relaxations of these solutions were measured using the benchtop magnetic relaxometer (B = 0.47 T mq 20) from Bruker. All measurements were performed in triplicate.

Cytotoxicity Assay. H9c2 and HeLa cells (2500 cells/well) were seeded in 96-well plates and incubated with the corresponding composite IO-PAA nanoprobes (35 μL, 28 mM in PBS pH 7.4) at 37 °C. After the specific time incubation, each well was washed three times with 1 × PBS and treated with 30 μL of MTT (2 μg/μL) for 2 h. The resulting formazan crystals were dissolved in acidic isopropyl alcohol (0.1 N HCl), and the absorbance was recorded at 570 and 750 nm (background), using a Synergy μQuant microtiter plate reader (Biotek). Experiments were performed in triplicate.

Conflict of Interest: The authors declare no competing financial interest.

Acknowledgment. This work was supported in part by NIH Grant GM084331 and UCF-NSTC Start Up Fund, all to J.M.P. This study was also partly supported by NIH Grant P30 CA008748-44 S5 and MSKCC Gerstner Young Investigator Award (to J.G.). We thank Dr. S. M. Hussain from the US Air Force's Wright-Patterson Air Force Base, Ohio, USA, for assistance with ICP-MS experiments.

Supporting Information Available: Detailed physical characterizations of the magnetic probes including dynamic light scattering (DLS), scanning transmittance electron microscopy (STEM), FT-IR, zeta-potential, stability of the nanoprobes at different conditions, MRI-based magnetic relaxations, encapsulating drug release, and cytotoxicity studies. This material is available free of charge *via* the Internet at http://pubs.acs.org.

REFERENCES AND NOTES

1. Winter, P. M.; Caruthers, S. D.; Wickline, S. A.; Lanza, G. M. Molecular Imaging by MRI. *Curr. Cardiol. Rep.* **2006**, *8*, 65–69.
2. Hu, X.; Norris, D. G. Advances in High-Field Magnetic Resonance Imaging. *Annu. Rev. Biomed. Eng.* **2004**, *6*, 157–184.
3. Aime, S.; Cabella, C.; Colombatto, S.; Geninatti Crich, S.; Gianolio, E.; Maggioni, F. Insights into the Use of Paramagnetic Gd(III) Complexes in MR-Molecular Imaging Investigations. *J. Magn. Reson. Imaging* **2002**, *16*, 394–406.
4. Louie, A. Multimodality Imaging Probes: Design and Challenges. *Chem. Rev.* **2010**, *110*, 3146–3195.
5. Mulder, W. J.; Strijkers, G. J.; Griffioen, A. W.; van Bloois, L.; Molema, G.; Storm, G.; Koning, G. A.; Nicolay, K. A Liposomal System for Contrast-Enhanced Magnetic Resonance Imaging of Molecular Targets. *Bioconjugate Chem.* **2004**, *15*, 799–806.
6. Mazooz, G.; Mehlman, T.; Lai, T. S.; Greenberg, C. S.; Dewhirst, M. W.; Neeman, M. Development of Magnetic Resonance Imaging Contrast Material for *In Vivo* Mapping of Tissue Transglutaminase Activity. *Cancer Res.* **2005**, *65*, 1369–1375.
7. Josephson, L.; Tung, C. H.; Moore, A.; Weissleder, R. High-Efficiency Intracellular Magnetic Labeling with Novel Superparamagnetic-Tat Peptide Conjugates. *Bioconjugate Chem.* **1999**, *10*, 186–191.
8. Caravan, P.; Ellison, J. J.; McMurry, T. J.; Lauffer, R. B. Gadolinium(III) Chelates as MRI Contrast Agents: Structure, Dynamics, and Applications. *Chem. Rev.* **1999**, *99*, 2293–2352.
9. Song, Y.; Zong, H.; Trivedi, E. R.; Vesper, B. J.; Waters, E. A.; Barrett, A. G.; Radosevich, J. A.; Hoffman, B. M.; Meade, T. J. Synthesis and Characterization of New Porphyrazine-Gd-(III) Conjugates as Multimodal MR Contrast Agents. *Bioconjugate Chem.* **2010**, *21*, 2267–2275.
10. Frullano, L.; Meade, T. J. Multimodal MRI Contrast Agents *J. Biol. Inorg. Chem.* **2007**, *12*, 939–949.
11. Tu, C. Q.; Louie, A. Y. Photochromically-Controlled, Reversibly-Activated MRI and Optical Contrast Agent. *Chem. Commun.* **2007**, 1331–1333.
12. Uzgiris, E. E.; Cline, H.; Moasser, B.; Grimmond, B.; Amaratunga, M.; Smith, J. F.; Goddard, G. Conformation and Structure of Polymeric Contrast Agents for Medical Imaging. *Biomacromolecules* **2004**, *5*, 54–61.
13. Endres, P. J.; MacRenaris, K. W.; Vogt, S.; Meade, T. J. Cell-Permeable MR Contrast Agents with Increased Intracellular Retention. *Bioconjugate Chem.* **2008**, *19*, 2049–2059.
14. Laurent, S.; Forge, D.; Port, M.; Roch, A.; Robic, C.; Vander Elst, L.; Muller, R. N. Magnetic Iron Oxide Nanoparticles: Synthesis, Stabilization, Vectorization, Physicochemical Characterizations, and Biological Applications. *Chem. Rev.* **2008**, *108*, 2064–2110.
15. Hu, F.; Macrenaris, K. W.; Waters, E. A.; Schultz-Sikma, E. A.; Eckermann, A. L.; Meade, T. J. Highly Dispersible, Superparamagnetic Magnetite Nanoflowers for Magnetic Resonance Imaging. *Chem. Commun.* **2010**, *46*, 73–75.
16. Cho, S. J.; Jarrett, B. R.; Louie, A. Y.; Kauzlarich, S. M. Gold-Coated Iron Nanoparticles: A Novel Magnetic Resonance Agent for T-1 and T-2 Weighted Imaging. *Nanotechnology* **2006**, *17*, 640–644.
17. Huber, M. M.; Staubli, A. B.; Kustedjo, K.; Gray, M. H.; Shih, J.; Fraser, S. E.; Jacobs, R. E.; Meade, T. J. Fluorescently Detectable Magnetic Resonance Imaging Agents. *Bioconjugate Chem.* **1998**, *9*, 242–249.
18. Hooker, J. M.; Datta, A.; Botta, M.; Raymond, K. N.; Francis, M. B. Magnetic Resonance Contrast Agents from Viral Capsid Shells: A Comparison of Exterior and Interior Cargo Strategies. *Nano Lett.* **2007**, *7*, 2207–2210.
19. Crich, S. G.; Biancone, L.; Cantaluppi, V.; Duo, D.; Esposito, G.; Russo, S.; Camussi, G.; Aime, S. Improved Route for the Visualization of Stem Cells Labeled with a Gd-/Eu-Chelate as Dual (MRI and Fluorescence) Agent. *Magn. Reson. Med.* **2004**, *51*, 938–944.
20. Brekke, C.; Morgan, S. C.; Lowe, A. S.; Meade, T. J.; Price, J.; Williams, S. C.; Modo, M. The *In Vitro* Effects of a Bimodal Contrast Agent on Cellular Functions and Relaxometry. *NMR Biomed.* **2007**, *20*, 77–89.
21. Anderson, E. A.; Isaacman, S.; Peabody, D. S.; Wang, E. Y.; Canary, J. W.; Kirshenbaum, K. Viral Nanoparticles Donning a Paramagnetic Coat: Conjugation of MRI Contrast Agents to the MS2 Capsid. *Nano Lett.* **2006**, *6*, 1160–1164.
22. Santra, S.; Kaittanis, C.; Grimm, J.; Perez, J. M. Drug/Dye-Loaded, Multifunctional Iron Oxide Nanoparticles for Combined Targeted Cancer Therapy and Dual Optical/Magnetic Resonance Imaging. *Small* **2009**, *5*, 1862–1868.
23. Chen, T.; Shukoor, M. I.; Wang, R.; Zhao, Z.; Yuan, Q.; Bamrungsap, S.; Xiong, X.; Tan, W. Smart Multifunctional Nanostructure for Targeted Cancer Chemotherapy and Magnetic Resonance Imaging. *ACS Nano* **2011**, *5*, 7866–7873.
24. Kim, H. M.; Lee, H.; Hong, K. S.; Cho, M. Y.; Sung, M. H.; Poo, H.; Lim, Y. T. Synthesis and High Performance of Magneto-fluorescent Polyelectrolyte Nanocomposites as MR/Near-Infrared Multimodal Cellular Imaging Nanoprobes. *ACS Nano* **2011**, *5*, 8230–8240.
25. Paquet, C.; de Haan, H. W.; Leek, D. M.; Lin, H. Y.; Xiang, B.; Tian, G.; Kell, A.; Simard, B. Clusters of Superparamagnetic

Iron Oxide Nanoparticles Encapsulated in a Hydrogel: A Particle Architecture Generating a Synergistic Enhancement of the T2 Relaxation. *ACS Nano* **2011**, *5*, 3104–3112.
26. Poselt, E.; Kloust, H.; Tromsdorf, U.; Janschel, M.; Hahn, C.; Masslo, C.; Weller, H. Relaxivity Optimization of a PEGylated Iron-Oxide-Based Negative Magnetic Resonance Contrast Agent for T(2)-Weighted Spin-Echo Imaging. *ACS Nano* **2012**, *6*, 1619–1624.
27. Tromsdorf, U. I.; Bigall, N. C.; Kaul, M. G.; Bruns, O. T.; Nikolic, M. S.; Mollwitz, B.; Sperling, R. A.; Reimer, R.; Hohenberg, H.; Parak, W. J.; *et al.* Size and Surface Effects on the MRI Relaxivity of Manganese Ferrite Nanoparticle Contrast Agents. *Nano Lett.* **2007**, *7*, 2422–2427.
28. Tu, C.; Ng, T. S.; Sohi, H. K.; Palko, H. A.; House, A.; Jacobs, R. E.; Louie, A. Y. Receptor-Targeted Iron Oxide Nanoparticles for Molecular MR Imaging of Inflamed Atherosclerotic Plaques. *Biomaterials* **2011**, *32*, 7209–7216.
29. Bae, K. H.; Kim, Y. B.; Lee, Y.; Hwang, J.; Park, H.; Park, T. G. Bioinspired Synthesis and Characterization of Gadolinium-Labeled Magnetite Nanoparticles for Dual Contrast T(1)- and T(2)-Weighted Magnetic Resonance Imaging. *Bioconjugate Chem.* **2010**, *21*, 505–512.
30. Bull, S. R.; Guler, M. O.; Bras, R. E.; Meade, T. J.; Stupp, S. I. Self-Assembled Peptide Amphiphile Nanofibers Conjugated to MRI Contrast Agents. *Nano Lett.* **2005**, *5*, 1–4.
31. Bull, S. R.; Guler, M. O.; Bras, R. E.; Venkatasubramanian, P. N.; Stupp, S. I.; Meade, T. J. Magnetic Resonance Imaging of Self-Assembled Biomaterial Scaffolds. *Bioconjugate Chem.* **2005**, *16*, 1343–1348.
32. Datta, A.; Hooker, J. M.; Botta, M.; Francis, M. B.; Aime, S.; Raymond, K. N. High Relaxivity Gadolinium Hydroxypyridonate-Viral Capsid Conjugates: Nanosized MRI Contrast Agents. *J. Am. Chem. Soc.* **2008**, *130*, 2546–2552.
33. Drake, P.; Cho, H. J.; Shih, P. S.; Kao, C. H.; Lee, K. F.; Kuo, C. H.; Lin, X. Z.; Lin, Y. J. Gd-Doped Iron-Oxide Nanoparticles for Tumor Therapy *via* Magnetic Field Hyperthermia. *J. Mater. Chem.* **2007**, *17*, 4914–4918.
34. Pan, D.; Caruthers, S. D.; Hu, G.; Senpan, A.; Scott, M. J.; Gaffney, P. J.; Wickline, S. A.; Lanza, G. M. Ligand-Directed Nanobialys as Theranostic Agent for Drug Delivery and Manganese-Based Magnetic Resonance Imaging of Vascular Targets. *J. Am. Chem. Soc.* **2008**, *130*, 9186–9187.
35. Song, Y.; Kohlmeir, E. K.; Meade, T. J. Synthesis of Multimeric MR Contrast Agents for Cellular Imaging. *J. Am. Chem. Soc.* **2008**, *130*, 6662–6663.
36. Song, Y.; Xu, X.; MacRenaris, K. W.; Zhang, X. Q.; Mirkin, C. A.; Meade, T. J. Multimodal Gadolinium-Enriched DNA-Gold Nanoparticle Conjugates for Cellular Imaging. *Angew. Chem., Int. Ed.* **2009**, *48*, 9143–9147.
37. Cheng, Z.; Thorek, D. L.; Tsourkas, A. Gadolinium-Conjugated Dendrimer Nanoclusters as a Tumor Targeted T1 Magnetic Resonance Imaging Contrast Agent. *Angew. Chem., Int. Ed.* **2010**, *49*, 346–350.
38. Cheng, Z. L.; Thorek, D. L. J.; Tsourkas, A. Porous Polymersomes with Encapsulated Gd-Labeled Dendrimers as Highly Efficient MRI Contrast Agents. *Adv. Funct. Mater.* **2009**, *19*, 3753–3759.
39. Allen, M. J.; MacRenaris, K. W.; Venkatasubramanian, P. N.; Meade, T. J. Cellular Delivery of MRI Contrast Agents. *Chem. Biol.* **2004**, *11*, 301–307.
40. Manus, L. M.; Mastarone, D. J.; Waters, E. A.; Zhang, X. Q.; Schultz-Sikma, E. A.; Macrenaris, K. W.; Ho, D.; Meade, T. J. Gd(III)-Nanodiamond Conjugates for MRI Contrast Enhancement. *Nano Lett.* **2010**, *10*, 484–489.
41. Mastarone, D. J.; Harrison, V. S.; Eckermann, A. L.; Parigi, G.; Luchinat, C.; Meade, T. J. A Modular System for the Synthesis of Multiplexed Magnetic Resonance Probes. *J. Am. Chem. Soc.* **2011**, *133*, 5329–5337.
42. Major, J. L.; Meade, T. J. Bioresponsive, Cell-Penetrating, and Multimeric MR Contrast Agents. *Acc. Chem. Res.* **2009**, *42*, 893–903.
43. Kalman, F. K.; Woods, M.; Caravan, P.; Jurek, P.; Spiller, M.; Tircso, G.; Kiraly, R.; Brucher, E.; Sherry, A. D. Potentiometric and Relaxometric Properties of a Gadolinium-Based MRI Contrast Agent for Sensing Tissue pH. *Inorg. Chem.* **2007**, *46*, 5260–5270.
44. Duimstra, J. A.; Femia, F. J.; Meade, T. J. A Gadolinium Chelate for Detection of Beta-Glucuronidase: A Self-Immolative Approach. *J. Am. Chem. Soc.* **2005**, *127*, 12847–12855.
45. Caravan, P.; Cloutier, N. J.; Greenfield, M. T.; McDermid, S. A.; Dunham, S. U.; Bulte, J. W.; Amedio, J. C., Jr.; Looby, R. J.; Supkowski, R. M.; Horrocks, W. D.; *et al.* The Interaction of MS-325 with Human Serum Albumin and Its Effect on Proton Relaxation Rates. *J. Am. Chem. Soc.* **2002**, *124*, 3152–3162.
46. Caravan, P. Strategies for Increasing the Sensitivity of Gadolinium Based MRI Contrast Agents. *Chem. Soc. Rev.* **2006**, *35*, 512–523.
47. Aime, S.; Castelli, D. D.; Crich, S. G.; Gianolio, E.; Terreno, E. Pushing the Sensitivity Envelope of Lanthanide-Based Magnetic Resonance Imaging (MRI) Contrast Agents for Molecular Imaging Applications. *Acc. Chem. Res.* **2009**, *42*, 822–831.
48. Tu, C.; Osborne, E. A.; Louie, A. Y. Activatable T1 and T2 Magnetic Resonance Imaging Contrast Agents. *Annu. Biomed. Eng.* **2011**, *39*, 1335–1348.
49. Major, J. L.; Parigi, G.; Luchinat, C.; Meade, T. J. The Synthesis and *In Vitro* Testing of a Zinc-Activated MRI Contrast Agent. *Proc. Natl. Acad. Sci. U.S.A.* **2007**, *104*, 13881–13886.
50. Zhang, X. A.; Lovejoy, K. S.; Jasanoff, A.; Lippard, S. J. Water-Soluble Porphyrins as a Dual-Function Molecular Imaging Platform for MRI and Fluorescence Zinc Sensing. *Proc. Natl. Acad. Sci. U.S.A.* **2007**, *104*, 10780–10785.
51. Louie, A. Y.; Huber, M. M.; Ahrens, E. T.; Rothbacher, U.; Moats, R.; Jacobs, R. E.; Fraser, S. E.; Meade, T. J. *In Vivo* Visualization of Gene Expression Using Magnetic Resonance Imaging. *Nat. Biotechnol.* **2000**, *18*, 321–325.
52. Urbanczyk-Pearson, L. M.; Meade, T. J. Preparation of Magnetic Resonance Contrast Agents Activated by Beta-Galactosidase. *Nat. Protoc.* **2008**, *3*, 341–350.
53. Frullano, L.; Tejerina, B.; Meade, T. J. Synthesis and Characterization of a Doxorubicin-Gd(III) Contrast Agent Conjugate: A New Approach toward Prodrug-Procontrast Complexes. *Inorg. Chem.* **2006**, *45*, 8489–8491.
54. Lee, J.; Burdette, J. E.; MacRenaris, K. W.; Mustafi, D.; Woodruff, T. K.; Meade, T. J. Rational Design, Synthesis, and Biological Evaluation of Progesterone-Modified MRI Contrast Agents. *Chem. Biol.* **2007**, *14*, 824–834.
55. Yang, H.; Zhuang, Y.; Sun, Y.; Dai, A.; Shi, X.; Wu, D.; Li, F.; Hu, H.; Yang, S. Targeted Dual-Contrast T1- and T2-Weighted Magnetic Resonance Imaging of Tumors Using Multifunctional Gadolinium-Labeled Superparamagnetic Iron Oxide Nanoparticles. *Biomaterials* **2011**, *32*, 4584–4593.
56. Perez, J. M.; Josephson, L.; O'Loughlin, T.; Hogemann, D.; Weissleder, R. Magnetic Relaxation Switches Capable of Sensing Molecular Interactions. *Nat. Biotechnol.* **2002**, *20*, 816–820.
57. Kaittanis, C.; Boukhriss, H.; Santra, S.; Naser, S. A.; Perez, J. M. Rapid and Sensitive Detection of an Intracellular Pathogen in Human Peripheral Leukocytes with Hybridizing Magnetic Relaxation Nanosensors. *PloS One* **2012**, *7*, e35326.
58. Kaittanis, C.; Santra, S.; Perez, J. M. Role of Nanoparticle Valency in the Nondestructive Magnetic-Relaxation-Mediated Detection and Magnetic Isolation of Cells in Complex Media. *J. Am. Chem. Soc.* **2009**, *131*, 12780–12791.
59. Kaittanis, C.; Santra, S.; Santiesteban, O. J.; Henderson, T. J.; Perez, J. M. The Assembly State between Magnetic Nanosensors and Their Targets Orchestrates Their Magnetic Relaxation Response. *J. Am. Chem. Soc.* **2011**, *133*, 3668–3676.
60. Haun, J. B.; Castro, C. M.; Wang, R.; Peterson, V. M.; Marinelli, B. S.; Lee, H.; Weissleder, R. Micro-NMR for Rapid Molecular Analysis of Human Tumor Samples. *Sci. Trans. Med.* **2011**, *3*, 71ra16.
61. Asati, A.; Santra, S.; Kaittanis, C.; Nath, S.; Perez, J. M. Oxidase-like Activity of Polymer-Coated Cerium

Oxide Nanoparticles. *Angew. Chem., Int. Ed.* **2009**, *48*, 2308–2312.
62. Asati, A.; Santra, S.; Kaittanis, C.; Perez, J. M. Surface-Charge-Dependent Cell Localization and Cytotoxicity of Cerium Oxide Nanoparticles. *ACS Nano* **2010**, *4*, 5321–5331.
63. Santra, S.; Kaittanis, C.; Perez, J. M. Aliphatic Hyperbranched Polyester: A New Building Block in the Construction of Multifunctional Nanoparticles and Nanocomposites. *Langmuir* **2010**, *26*, 5364–5373.
64. Lattuada, L.; Lux, G. Synthesis of Gd-DTPA-Cholesterol: A New Lipophilic Gadolinium Complex as a Potential MRI Contrast Agent. *Tetrahedron Lett.* **2003**, *44*, 3893–3895.
65. Weinmann, H. J.; Brasch, R. C.; Press, W. R.; Wesbey, G. E. Characteristics of Gadolinium-DTPA Complex: A Potential NMR Contrast Agent. *Am. J. Roentgenol.* **1984**, *142*, 619–624.
66. McCarthy, J. R.; Perez, J. M.; Bruckner, C.; Weissleder, R. Polymeric Nanoparticle Preparation That Eradicates Tumors. *Nano Lett.* **2005**, *5*, 2552–2556.
67. Sun, E. Y.; Josephson, L.; Weissleder, R. "Clickable" Nanoparticles for Targeted Imaging. *Mol. Imaging* **2006**, *5*, 122–128.
68. Perez, J. M.; Asati, A.; Nath, S.; Kaittanis, C. Synthesis of Biocompatible Dextran-Coated Nanoceria with pH-Dependent Antioxidant Properties. *Small* **2008**, *4*, 552–556.